JOURNAL OF CATALYSIS 54, 303–317 (1978)

A Study of Pyridine Adsorbed on Silica–Alumina Catalysts by Combined Infrared Spectroscopy and Temperature-Programmed Desorption

J. A. SCHWARZ,[1] B. G. RUSSELL, AND H. F. HARNSBERGER[2]

Chevron Research Company, Richmond, California 94802

Received September 8, 1977; revised May 10, 1978

A combined technique employing transmission infrared spectroscopy (IR) and temperature-programmed desorption (TPD) has been used to study the interaction of a gaseous base with a series of acidic microporous catalyst surfaces. This technique was used to establish the first-order kinetics for pyridine desorption from silica–alumina gel catalysts covering a wide range of compositions. This combined technique has also allowed more detailed information about number, type, and strength of acid sites on catalysts to be obtained in a single experiment. The special measuring system that allows simultaneous transmission infrared monitoring and temperature-programmed desorption from catalysts is described. The results of applying this combined technique to a model silica–alumina catalyst system are shown. Insight into the mechanism for the desorption of both Lewis and Brønsted chemisorbed pyridine was deduced from the TPD results. A model for pyridine desorption is presented and discussed.

INTRODUCTION

The concept of "active centers" on catalytic surfaces was first introduced by H. S. Taylor in 1925. The existence and chemical nature of such sites has been examined extensively over the past five decades. A large number of catalytic reactions have indeed been identified as taking place on special groups of sites, which in some cases represent only a small fraction of the total number available on the surface.

Various techniques are used to obtain information on the nature, activity, number, and type of active sites on catalysts. Among these are transmission infrared spectroscopy (IR) and temperature-programmed desorption (TPD). IR has been used extensively to study and characterize supported catalysts for more than a decade. IR surface studies, initially by R. P. Eischens and others, have contributed much to our understanding of surface and sorbed species and of gas–solid catalytic reactions. The infrared spectrum of a simple molecule arises as a result of the vibrations of the atoms within the molecule; the symmetry and bond strengths of the molecule as a whole determine the number and frequencies of the vibrations. When a simple molecule is adsorbed, the "one-sided" surface forces exerted by a catalytic material must cause a change in symmetry of the molecule; any quantitative measure of this change can be directly related to the nature of the adsorption.

It has long been known that certain

[1] Present address: Exxon Research and Engineering Company, P.O. Box 45, Linden, New Jersey 07036.

[2] To whom correspondence should be addressed.

0021-9517/78/0543-0303$02.00/0

gaseous bases which selectively adsorb (under the proper conditions) on acidic surface sites can give rise to IR spectra that can characterize the type of acid site present on the catalytic surface. Pyridine is such a gaseous base, and it has been used successfully in combination with IR to determine the number and type of acid sites present on oxide surfaces (*1–6*).

Although adsorption of such bases as pyridine has demonstrated the utility of "titrating" catalytic surfaces to assess their chemical reactivity, less attention has been focused on the strength of the active acid center. Weak acid sites will not adsorb the gaseous pyridine; thus, the technique of gaseous base adsorption for characterization of catalyst acidity must be qualified by stipulating the type of titer used until a more detailed knowledge of the acid–base interaction is known.

Temperature-programmed desorption of chemisorbed molecules has been used successfully, especially by Cvetanovic and Amenomiya (*7*), to probe the binding strength of molecules on both oxide and metal catalyst surfaces. Some of the catalytic applications include (a) ethylene on alumina and silica–alumina and (b) hydrogen on transition metals. For most gas–solid systems, chemisorption occurs in several states, each with a discrete binding energy. Temperature-programmed desorption has been used to determine the values of these binding energies by heating a surface after exposure to a gas and observing the temperature range over which the gas is desorbed.

If the desorbing gas has interacted with specific sites on the catalytic surface (e.g., gaseous base adsorbing on acid sites) during the adsorption, then the TPD spectra provides information about the binding of this probe-gas on the active surface sites. Thus, a measure of the acid strength can be obtained when a gaseous base is the adsorbate. Recently, Takahashi *et al.* (*15*) have used thermal desorption of pyridine and *n*-butylamine to study the acid sites on commerical silica–alumina cracking catalysts.

We describe the measuring system which combines (a) infrared analysis of surface-adsorbed species and (b) infrared characterization of surface activity with (c) mass spectrometric determination of catalytic activity. The application of this combined technique to the study of three experimental silica–alumina gel catalysts will also be described.

BACKGROUND INFORMATION

Infrared

A considerable amount of research has been done to study the interaction of pyridine with high area catalytic supports (*1–5*). Parry (*1*) has identified the adsorption levels of pyridine which correspond not only to the molecules chemisorbed on acid sites, but also to those molecules bound by physical adsorption and hydrogen bonded to the surface. Moreover, the condition that determines only chemisorption on acid sites was established. Recently, one of us (J.A.S.) developed a method which permitted simultaneous determination of the site densities of Lewis and Brønsted acids for a series of silica–alumina gels (*6*). In earlier work, there has been considerable success using IR techniques to assess the total number of acid sites present on a catalyst by titrating the surface with a suitable vapor base. This procedure involved dosing a sample with small known amounts of pyridine vapor at 150°C and recording the IR spectrum. The band area that corresponds to saturation exposure is, thus, related to the total acidity of the surface. Until recently, when both Lewis and Brønsted sites were present, this method was not possible, for there was no general way of establishing how the gaseous base partitioned itself between the two types of chemisorbing sites. However, the two-step modified pyridine titration de-

veloped by Schwarz permits a quantitative measure of the number of both Lewis and Brønsted acid sites on solid catalysts. This is achieved without having to use independent calibrations or absorption coefficients.

Temperature-Programmed Desorption

After exposure of a sample to a known amount of pyridine and applying a known heating schedule to the sample, the none steady-state surface coverage of pyridin- is determined by

$$N(t) = \frac{-d\sigma}{dt} = \nu_n \sigma^n \exp[-E^{\neq}/RT(t)], \quad (1)$$

where $N(t)$ is the rate for desorption (molecules/cm² sec); σ is the surface coverage (molecules/cm²) as measured by IR; n is the kinetic order for the desorption process; ν_n is the frequency factor for desorption; $E^{\neq}$ is the activation energy of desorption (cal/mole).

We will consider only a linear change of sample temperature with time $T = T_0 + \beta t$, where β is the constant heating rate in degrees Kelvin per second and t is heating time in seconds.

Equation (1) assumes that readsorption onto the sample is negligible and that no other processes impede the desorption of gas from the sample. The cases of finite readsorption and diffusion of the desorbed gas in the pores of the catalyst have been treated by Cvetanovic and Amenomiya (7). They showed that analysis of the temperature programmed desorption data using Eq. (1) is qualitatively similar even in these special cases. It is more than likely that if readsorption or diffusion is controlling the desorption reaction, it would not be detected experimentally because the diagnostic tests for these cases cannot be distinguished from one another within the usual experimental accuracy. Therefore, the standard analysis that has been presented in detail by Redhead (*8*), Ehrlich (*9*), and later Cvetanovic and Amenomiya (*7*) to the desorption curves, $N(t)$, can at best distinguish the order of the desorption event, n.

However, we show later that simultaneous monitoring of the surface coverage of pyridine (σ) and the gas phase pyridine during the desorption cycle allows for a semiquantitative evaluation of the mechanism for the desorption processes.

EXPERIMENTAL

Apparatus

The vacuum infrared catalyst cell, gas inlet manifold, sample holder and heater configuration, and operation of the Perkin–Elmer Model 180 IR spectrometer have been described by Ryason (*10*). Appendix I provides a practical guide to our IR wafer fabrication, mounting, installation, and subsequent IR analysis that is consistent with the high-vacuum well-controlled conditions possible in the IR measuring cell. The additional mass spectrometric facilities for monitoring the gas phase composition in the IR cell will now be described.

Figure 1 is a photograph of the combined infrared–mass spectrometric (IR–MS) measuring system. Figure 2 is a schematic for the system which specifies the various pumping facilities, valves, and other features of the ultrahigh-vacuum gas analysis region. The IR cell is joined to the mass spectrometer by a transfer line that carries gas directly into the ionizer of a UTI Model 100C quadrupole mass spectrometer. This mass spectrometer was chosen for its high sensitivity, long-term stability, and mass analysis range m/e 1 to m/e 500. The mass spectrometer uses a channeltron electron multiplier rather than the more conventional Be–Cu electron multiplier. The reason for this choice was the sta-

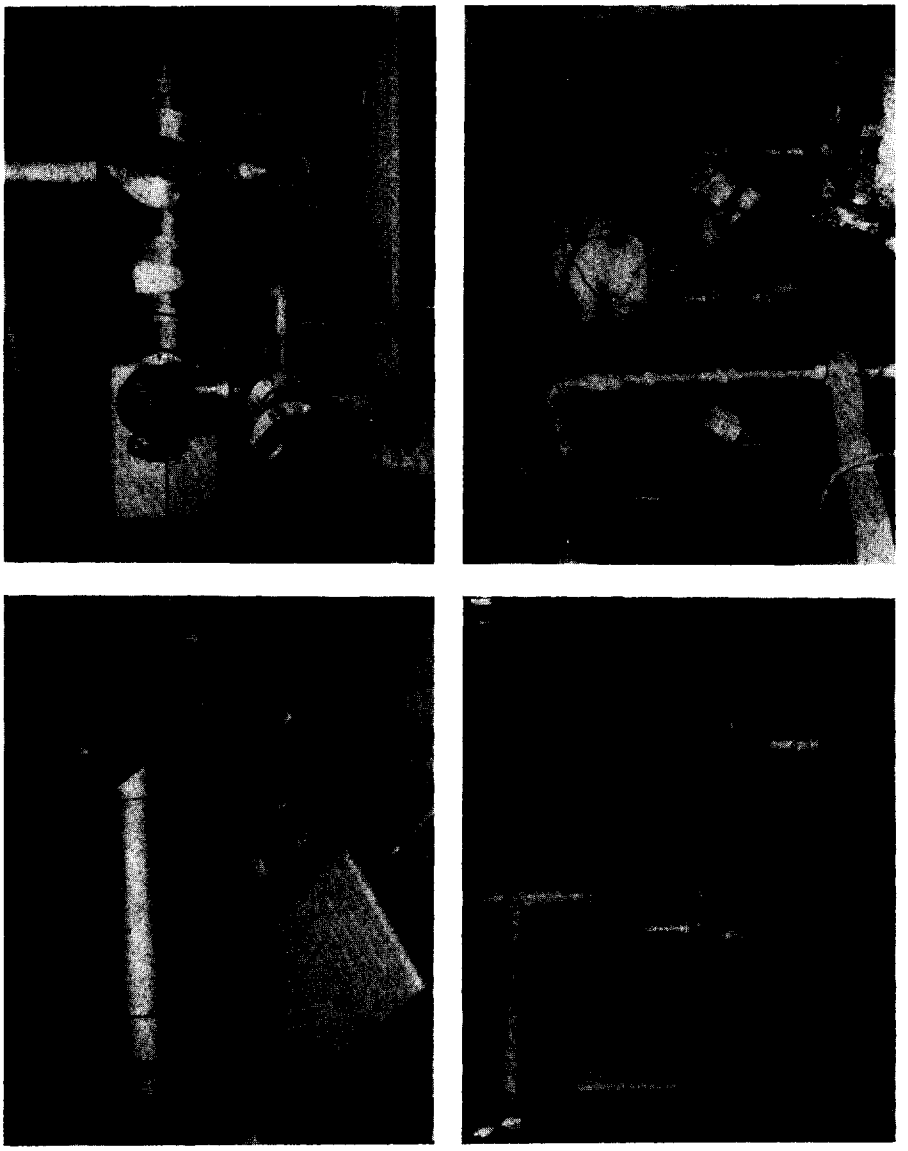

FIG. 1. Composite photo of IR–MS system.

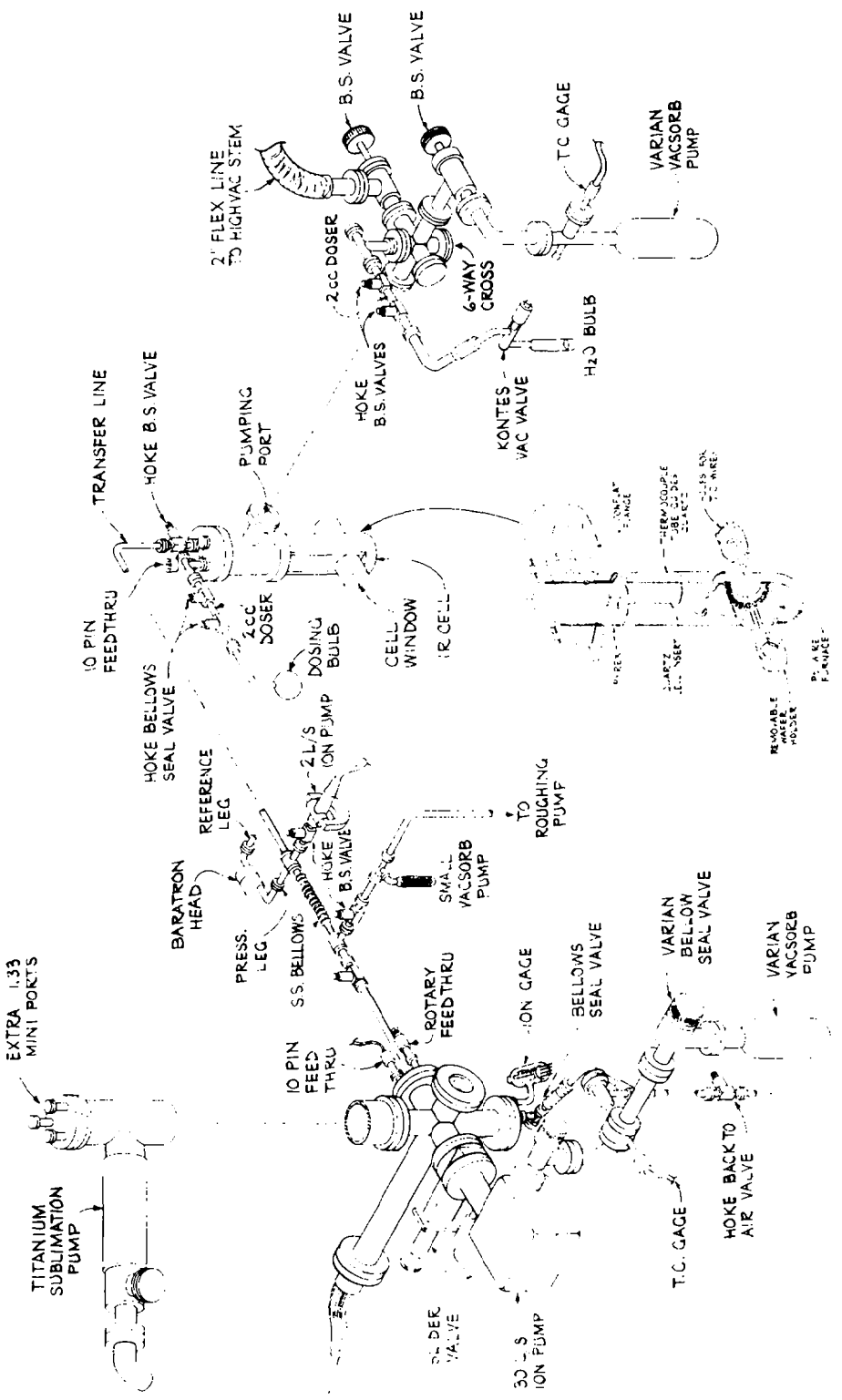

FIG. 2. Schematic of IR–MS unit.

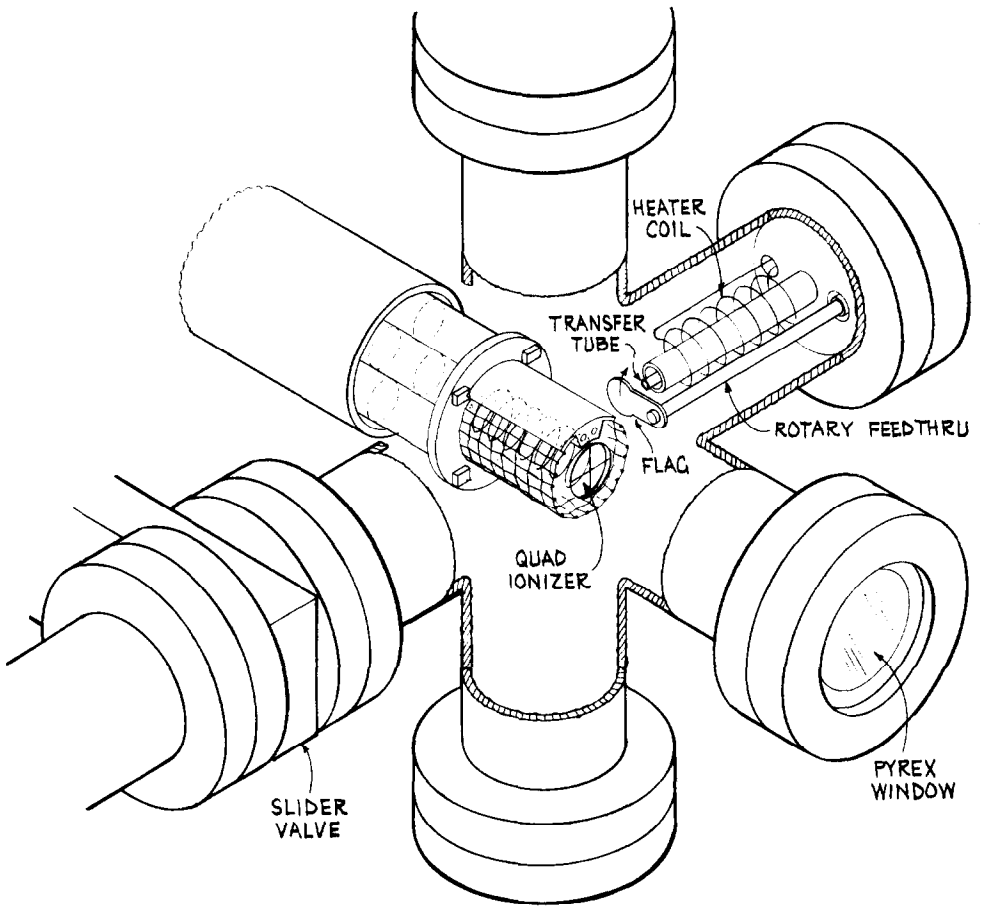

FIG. 3. UHV–MS chamber.

bility in systems which predominantly monitor hydrocarbons.

UHV System

The mass spectrometer is positioned in a special vacuum fitting made by Varian Associates. The center of the ionizer is located on the intersection of the center lines for each of the side ports of the "double-cross" vacuum fitting. Figure 3 depicts this ultrahigh-vacuum chamber. The system, which is portable, is rough pumped by a Vacsorb pump, which can be isolated from the UHV system by a Viton-seated valve. UHV conditions are obtained by a 30 liter/sec noble ion pump (Varian Model No. 911-5032) and a water-cooled titanium sublimation pump (TSP) (Varian Model No. 916-0033). The base pressure readily achieved in the UHV chamber after a mild bake (150°C) is $\sim 10^{-10}$ Torr (1 Torr = 133.3 N m^{-2}).

The Varian double-cross was designed to provide the maximum flexibility for the portable UHV system. In addition to the features mentioned, it also contains (see Fig. 3) an ionization gauge, window, heated gas inlet tube, and "flag" assembly that is used to discriminate between the gas transferred from the IR cell and the partial pressure of that gas in the UHV system. In addition, above the TSP (see Fig. 2) is a conflat flange with three mini-conflat inlets. The heater for the segment

of transfer tubing inside the UHV chamber is controlled by an ultrastable dc power supply (Hewlett–Packard Model No. 6264B) and an API controller (Research, Inc., Model No. 640). This provides stable power to the heater once thermal equilibrium is reached. The choice of dc heating was to eliminate any cross-coupling between the mass spectrometer and the heater supply.

Transfer Line

The transfer line connects the IR cell to the UHV chamber. The transfer tube begins in the IR cell with a Kovar tube (i.d. = 2.63 mm) that is silver soldered through a double-sided mini-conflat flange attached to one of the access ports of the IR cell. This tube extends into the IR cell and terminates ~1 mm from the catalyst sample surface. Thus, a considerable portion of the gas emitted from the catalyst wafer flows directly into the transfer tube. On the other side of the double conflat flange is a Hoke valve; following a gas path to the UHV system, the construction consists of a 0.5-in. tube, mini-conflat tee, bellows, another double-sided mini-conflat with a side-bored tube extending to the rough pumping systems for the transfer tube, another Hoke valve, and a double-sided mini-conflat with a welded tube that extends into the UHV system. This tube can be heated as described. A similar heating supply is provided for the portion of the transfer tube that enters the IR cell.

The transfer tube must be held at a low enough pressure to enable molecule–molecule collision-free gas flow from the IR cell to the UHV system. Connected to the mini-conflat tee is another Hoke valve and a 2-liter/sec mini-ion pump (Varian Model No. 913-5000). The base pressure in the transfer tube, when it is isolated from the IR cell, is $\sim 10^{-8}$ Torr. The transfer line is rough pumped through the side tube connected to the double-sided mini-conflat mentioned previously. Figure 2 shows the transfer line and associated pumping. The entire transfer line, valves, ion pump, and roughing line are wrapped with heating tape which is maintained at a temperature of 75 to 80°C.

Linear Temperature Programmer and System Response Time

The quartz furnace that surrounds and supports the catalyst wafer in the IR cell can be heated to a maximum temperature of ~850°C (*10*). A linear temperature programmer is applied to the heater wires to perform the thermal desorption experiments. The sample thermocouple is monitored as a function of time. It also provides an output to drive the X-axis of any X–Y recorder to obtain the thermal desorption spectrum.

Two other thermocouples positioned close to the wafer permit instantaneous monitoring of the sample temperature. Thermal gradients of ~20°C occur for temperatures <250°C, but become less (~10°C) as the wafer temperature is increased.

During a desorption experiment, the IR cell is isolated from the ion pump attached to the cell manifold. The cell is pumped by a high-speed trapped mechanical pump and well-chilled Vacsorb pump. Although the total pressure is rather high in the cell ($\sim 5 \times 10^{-4}$ Torr), the pumping speed for pyridine is extremely fast. When 2 μmole of pyridine is admitted to the cell from the doser, the cell pressure returns to its base value in ~10 sec, as determined by a Baratron pressure gauge connected to the cell; this amount of pyridine represents more gas than is generated during any desorption experiment. The pressure in the transfer line and UHV system responds similarly during these pulse experiments. The maximum heating rate used is 80°C/min. The characteristic pumping time $t = V/S$ (where V is the volume and S is the pumping speed for pyridine) approaches

0, and the partial pressure of pyridine measured by the quadrupole MS is proportional to the desorption rate (*8*).

Mass Spectrometric Detection of Pyridine

Attached to the roughing line for the transfer tube is a Cajon tee, which permits coupling of a thermostatted bulb containing reagent-grade, well-degassed pyridine. Pyridine at low pressure could be leaked into the UHV system, and the cracking pattern of the gas could be determined. The major peak was *m/e* 51. The flag assembly enabled accurate discrimination between gas coming through the transfer tube and background gas in the mass spectrometer chamber. The same ratio between pyridine mass peaks was measured when pyridine from the IR cell (with the catalyst present at 500°C) was directed through the transfer line into the UHV system. This shows that no cracking of the pyridine took place over the silica–alumina gel catalysts under our experimental conditions. It also means that little or no coke was deposited on the catalysts. All thermal desorption spectra up to 500°C were obtained for *m/e* 51, the major pyridine fragment generated in the quadrupole MS ionizer.

Sample Preparation

The experimental silica alumina gel catalysts used in this study were from the same batch of materials that was examined previously by the modified pyridine titration (*6*).

The adsorption–desorption studies were carried out on three silica–alumina gel samples, the compositions of which are given in Table 2. The samples were prepared by mixing the desired amounts of $AlCl_3$ and tetraethylorthosilicate in methanolic solution (*11*). The resulting solution was homogeneously gelled by the addition of propylene oxide, thus raising the pH. The methanol was then displaced by rinsing in diethyl ether. The resulting mixture was placed in an autoclave brought to the critical temperature of the diethyl ether. The vapor was flushed away with dry nitrogen. This resulted in an extremely high surface area material. XRF-determined chloride levels of the fresh material was 0.7 wt% Cl. Electron microprobe scans showed uniform spatial distribution of this Cl. Samples calcined, however, at 500°C had very low chloride levels, <0.03 wt% Cl. Self-supporting wafers of 5 to 7 mg and $\frac{1}{2}$-in. in diameter were pressed at low pressure (see Appendix I) and placed in the IR cell. The wafer was then calcined at 500°C for 1 hr in 160 Torr of O_2 before each experiment.

EXPERIMENTAL PROCEDURE

Each of the *in situ* calcined samples was subjected to the modified pyridine titration (*6*). This involved dosing each wafer with a known amount of pyridine. The IR spectrum was measured after each dosing at 150°C and $\sim 10^{-4}$ Torr pressure. Then, the pyridine was thermally desorbed at 80°C/min and the TPD spectrum was recorded up to 550°C. The peak height of IR bands characteristic of Lewis and Brønsted acidity (at 1450 and 1540 cm^{-1}, respectively) were, likewise, monitored during the desorption cycles. The wafer was then recalcined at 500°C for 45 min in 160 Torr of O_2 until it was carbonfree. Then the next stage of the pyridine titration was performed. After pyridine saturation (the sample equilibrated at 150°C in 4 Torr of pyridine, then pumped to 10^{-4} Torr pressure) and the 80°C/min TPD, the same cycle of experiments was performed, but at lower heating rates: ~30 and ~13°C/min. Thus, from each sample we have data characteristic of (a) constant surface coverage at variable heating rate and (b) constant heating rate at variable surface coverage. Saturation pyridine coverage was determined from the appropriate integrated IR band area and measured IR absorption coefficient (*6*).

TABLE 1

Temperatures for Maximum Pyridine Desorption Rate at Various Heating Rates and Surface Coverage

Sample	Surface condition	Heating rate (°C/min)	T_m (°K) by IR–TPD	T_p (°K) by MS–TPD
10 (by wt) SiO_2/ 90 (by wt) Al_2O_3	Exposure[a]	80	670	808
	Exposure	30	531	700
	Exposure	13	478	610
	One dose[b]	80	673	800
	Two doses	80	673	785
50 (by wt) SiO_2/ 50 (by wt) Al_2O_3	Exposure	80	595	746
	Exposure	30	548	650
	Exposure	13	495	570
	One dose	80	595	753
	Two doses	80	595	746
90 (by wt) SiO_2/ 10 (by wt) Al_2O_3	Exposure (Lewis)	80	528	625
	Exposure (Brønsted)	80	564	625
	Exposure	30	498	603
	Exposure	13	480	550
	Two doses	80	523	631

[a] Exposure represents 4 Torr pyridine.
[b] One dose represents 0.5 μmole of pyridine.

RESULTS

Figure 4 shows a typical set of raw data obtained by the above-mentioned procedure applied to the 10 wt% SiO_2/90 wt% Al_2O_3 sample for a heating rate of 43°C/min. The 1450-cm^{-1} band (Lewis acid) is shown. The IR desorption data were digitized, and the derivative of the decreasing surface concentration (net IR peak height) with respect to time was determined numerically. Equation (1) predicts that an Arrhenius plot of the IR data should be a straight line, depending on the order of the desorption rate (n = 0, 1, or 2). Figure 5 shows an example of the data obtained from the 50 wt% SiO_2/50 wt% Al_2O_3 sample. The best straight line is obtained for a first-order process (n = 1). Figures 6 and 7 show the IR data for n = 1 obtained under various coverages and heating rates for the 10 wt% SiO_2/90 wt% Al_2O_3 and 90 wt% SiO_2/10 wt% Al_2O_3, respectively. Note the latter sample showed the presence of both Lewis and Brønsted acid sites. Assuming that equilibration of the sample in 4 Torr of pyridine represents

TABLE 2

Pyridine Acid Titers and Desorption Activation Energies

Sample	SiO_2/Al_2O_3 (by wt)	Surface area (m^2/g)	Acid titer (IR) (pyridine ads. at 150°C, 10^{-4} Torr)		$E^{\neq}_{DES}$ (kcal/mole)	
			Lewis (μmole/m^2)	Brønsted (μmole/m^2)	By IR–TPD	By MS–TPD
I	10/90	630	0.55	0.00	8.4	8.3
II	50/50	570	0.65	0.00	6.0	5.4
III	90/10	740	0.23	0.044	5.3 Lewis 7.2 Brønsted	

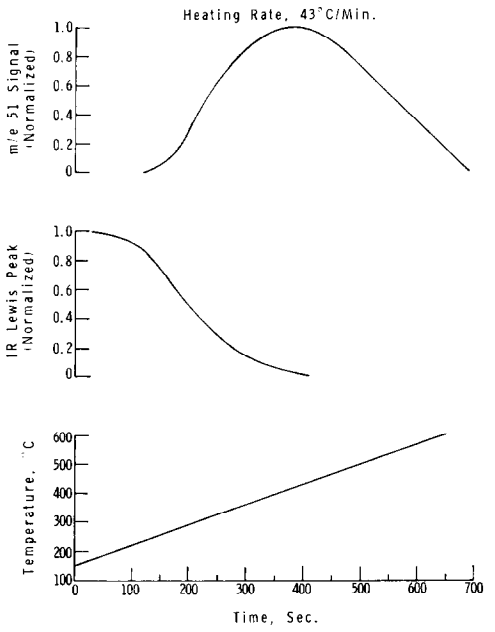

FIG. 4. MS, IR, and temperature versus desorption time for 10 wt% SiO_2/90 wt% Al_2O_3.

a saturation pyridine coverage, normalized desorption spectra (obtained by IR or MS) for pyridine doses less than saturation were normalized to that for saturation coverage. These are shown in Figs. 8, 9, and 10. Here, we plotted the "normalized desorption flux" (net mass spectrometer intensity at m/e 51 normalized to its value at T_P) as a function of the reduced temperature, T/T_P. T_P is the temperature at which the desorption flux was a maximum. Each sample gave a T_P that was independent of coverage at a constant heating rate, although T_P varied from sample to sample. These temperatures are shown in the legends to Figs. 8, 9, and 10, along with the coverage determined from the modified pyridine titration technique (*6*) applied to each sample. Note that the normalized desorption flux at $T = T_P$ agrees well with the independently determined coverage from the IR. These are further indications that the desorption kinetics for each silica–alumina sample are first-order in pyridine coverage. Figure 11 shows how the peak temperature varies with heating rate for a constant coverage on the 10 wt% SiO_2/90 wt% Al_2O_3 sample. The peak temperature decreases with decreasing heating rate, as predicted (*8*) for a first-order desorption.

We note now and discuss further later that Eq. (1) predicts that the maximum in the desorption flux should correspond to the maximum in the change in the surface concentration ($d\sigma/dt$ = maximum). Figure 5 shows that for $n = 0$, $d\sigma/dt$ is a maximum at $T = T_m = 600°K$. This does not correspond to $T = T_P$ (=750°K), as determined from the thermal desorption spectrum. This was true for all the samples, and a compilation of these temperature maxima for each of the samples and the experimental conditions are shown in Table 1. A qualitative explanation of these results, based on diffusion through the pore structure of the catalyst, is presented in the next section.

DISCUSSION

We found that: (a) Arrhenius plots of the IR data for pyridine adsorbed on both

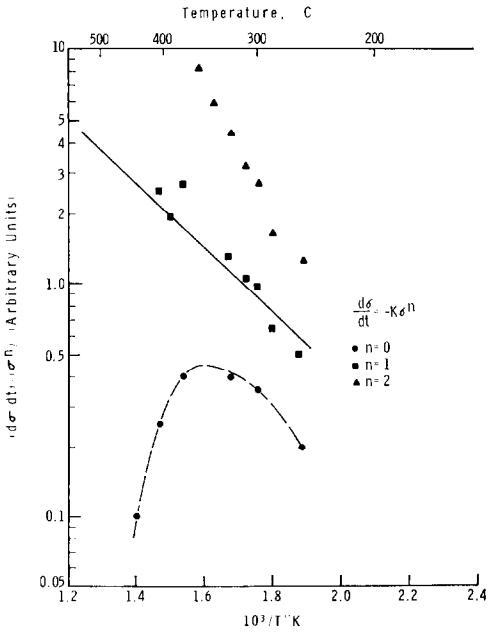

FIG. 5. Temperature dependence of IR band for Lewis adsorbed pyridine on 50% SiO_2/50% Al_2O_3.

Lewis and Brønsted acids are linear for $n = 1$ [see Eq. (1)]; (b) peak temperatures, T_m and T_p, are independent of surface coverage at a constant heating rate for each of the samples; (c) $\ln \beta/T_p^2$ versus $1/T_p$ was found to be linear for each series of thermal desorption spectra obtained; and (d) the surface coverage at $T = T_m$ (obtained from $d\sigma/dt$ = maximum) is approximately σ_p/e as predicted for a first-order desorption (*9*), where σ_p is the intensity of appropriate IR band at the start of the TPD measurement, i.e., at 150°C. Each of these observations is consistent with first-order desorption kinetics for pyridine adsorbed on either Lewis or Brønsted acid sites. Table 2 shows the activation energies ($E^{\neq}_{DES}$) determined from the IR–TPD and from the MS–TPD data obtained for each of the three gel samples. Included in Table 2 are Lewis and Brønsted acid site densities obtained from the IR–pyridine chemisorption at 150°C, 10^{-4} Torr. There is a systematic decrease in the binding energy of pyridine adsorbed on Lewis sites as the silica content is increased. Pyridine is bound to Brønsted acid sites in Sample III with a binding energy that is 27% larger than that of the Lewis acid-bound pyridine.

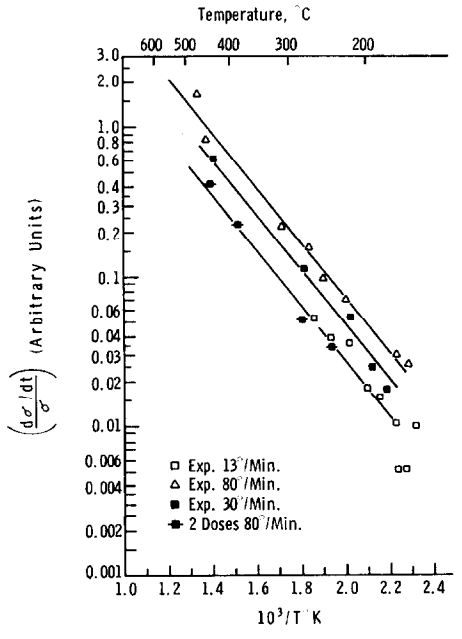

FIG. 6. Temperature dependence of IR band for Lewis acid adsorbed pyridine on 10% SiO_2/90% Al_2O_3.

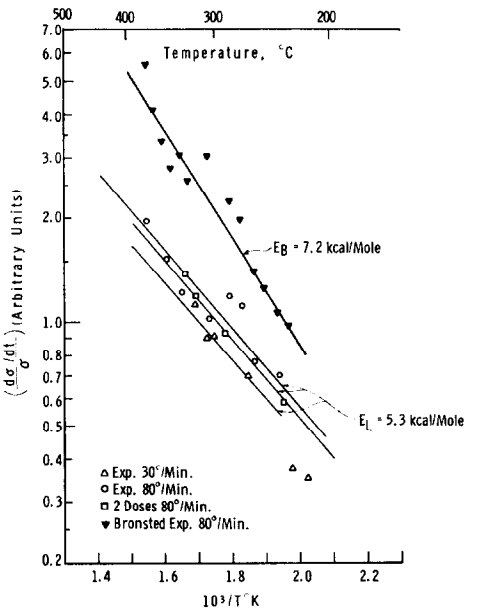

FIG. 7. Temperature dependence of IR band for Lewis and Brønsted adsorbed pyridine on 90% SiO_2/10% Al_2O_3.

The Brønsted site density determined from the IR pyridine chemisorption is quite low and presumably accounts for the lack of structure found in a thermal desorption spectra when more than one binding state of an adsorbed molecule is present.

Cvetanovic (*7*) treated the case of a gas that was thermally desorbed from a microporous sample and subsequently diffused through the pores of the catalyst. His numerical simulation has shown that the diagnostics used to establish the order of the desorption were still valid in this special case of pore diffusion. Thus, activation energies determined from the thermal desorption spectra, as we have shown here, are accurately determined by the characteristic plots (Figs. 6 and 7). Good agreement was obtained for desorption activation

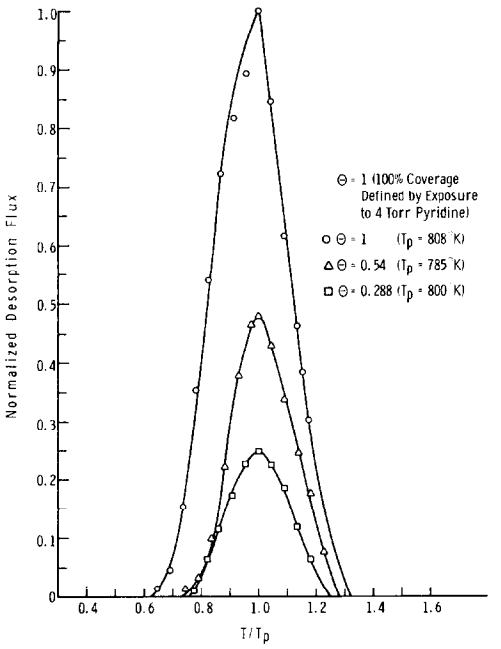

FIG. 8. Pyridine desorption from 10 wt% SiO_2/90 wt% Al_2O_3, constant heating rate, variable coverage.

energies calculated from (a) the IR spectra and (b) the MS data in a temperature-programmed pyridine desorption analysis. (See Table 2). We would expect that water partial pressure, P_{H_2O}, would have a significant effect on the concentration of Brønsted and Lewis sites during TPD experiments because thermal dehydration converts Brønsted to Lewis sites. TPD experiments at several fixed P_{H_2O} levels would provide more quantitative information on the effect of P_{H_2O}.

The binding energies of pyridine on these silica–aluminas are low. The characteristic parameter for determining the desorption profile is the parameter $E^{\neq}/RT_p$. For values of $E^{\neq}/RT_p < 10$, as pointed out (*8*), the approximations made in deriving the expression for the desorption profiles are not strictly valid. These approximations do not have to be made, if one uses tabulated values of the exponential integral to determine $N(t)$ in Eq. (1). For $E^{\neq}/RT_p < 10$, the normalized thermal desorption spectra are extremely broad (~200°C). Figure 12 shows the normalized desorption spectra for $\sigma = 1$ and $\beta = 80$°C/min on Sample I. However, it is noteworthy that the theoretical curve fits the experimental data quite well.

Two interesting features of our thermal desorption results remain to be discussed. They are: (1) the low value we obtained for $E^{\neq}$ and (2) the fact that $T_p - T_m \neq 0$ for any of the supports studied. We cannot rule out a coverage-dependent activation energy for desorption to explain our low value for the desorption energy, $E^{\neq}$. In modeling the diffusion process through a porous material, Cvetanovic did not include this as a possibility. However, earlier works (*12*) which have measured equilibrium adsorption isotherms and calorimetric heats of adsorption of various gaseous bases on well-degassed silica–alumina have shown heats of adsorption that vary with coverage, but the average value of the heat of adsorption does not change substantially from the value at zero coverage. In addi-

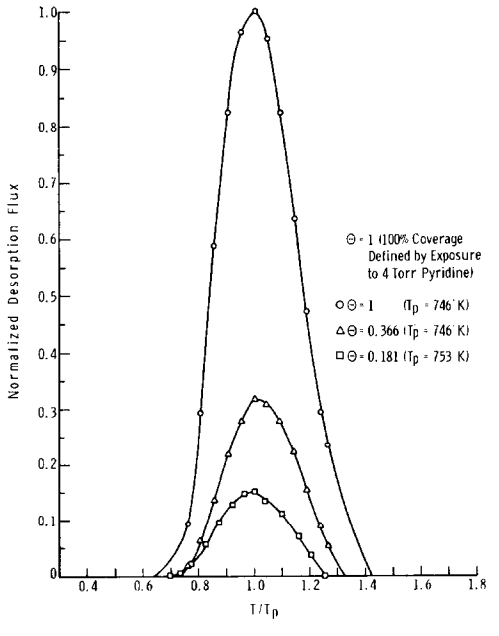

FIG. 9. Pyridine desorption from 50 wt% SiO_2/50 wt% Al_2O_3, constant heating rate, variable coverage.

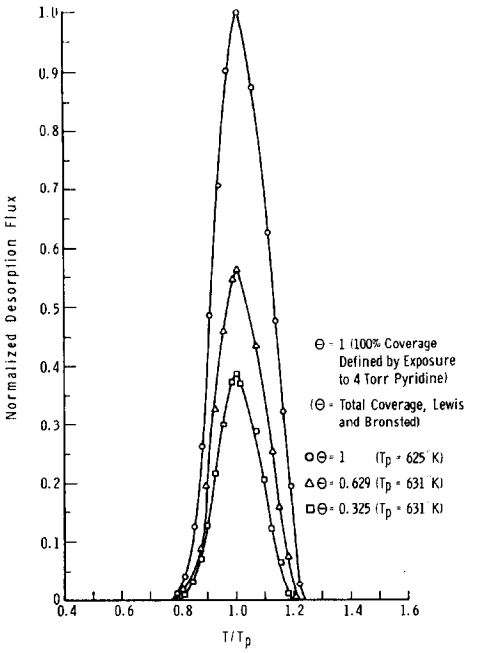

FIG. 10. Pyridine desorption from 90 wt% SiO_2/10 wt% Al_2O_3, constant heating rate, variable coverage.

tion, site density distribution functions determined from the adsorption data show remarkably narrow desorption energy site densities. That still leaves us with the fact that the activation energy for desorption of pyridine from these gels is lower than expected for a gaseous base adsorbed on a strong acid catalyst. Recent measurements of the heat of adsorption of pyridine (*13*) from solution, onto well-degassed silica–alumina supports gave values of the heats of physiosorption and chemisorption of pyridine as 11.3 and 22 kcal/mole, respectively. These values would appear to be more consistent with acid–base interaction energies. Yet earlier work (*14*) of gaseous pyridine adsorption on commercial silica–alumina catalysts gave values of the heat of adsorption of 3 to 4 kcal/mole, which agrees quite well with the desorption energies that we measure. However, in this earlier work it was concluded that diffusion was rate-limiting. This was due to

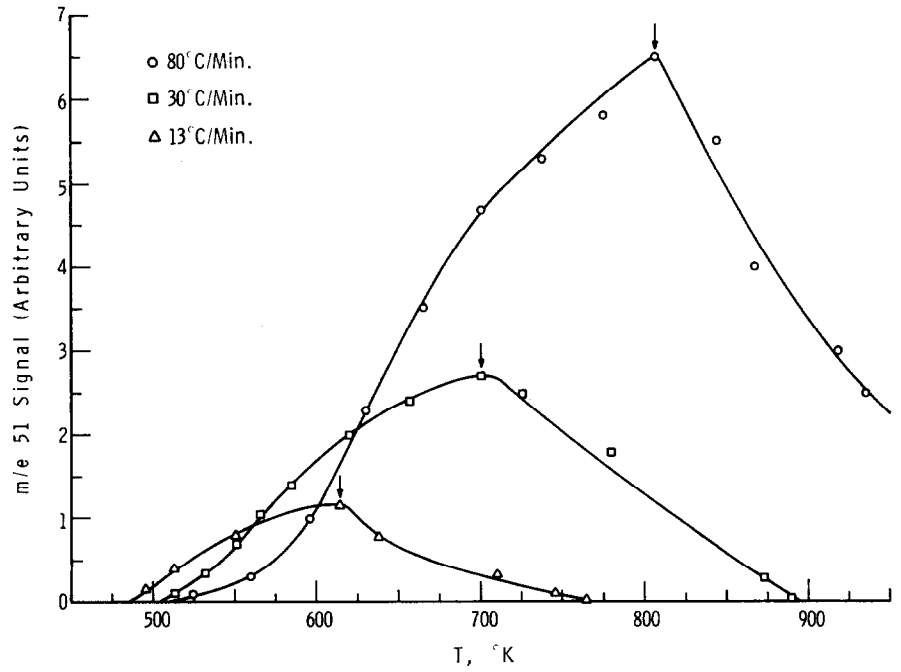

FIG. 11. Pyridine desorption from 10 wt% SiO_2/90 wt% Al_2O_3, variable heating rate, constant coverage.

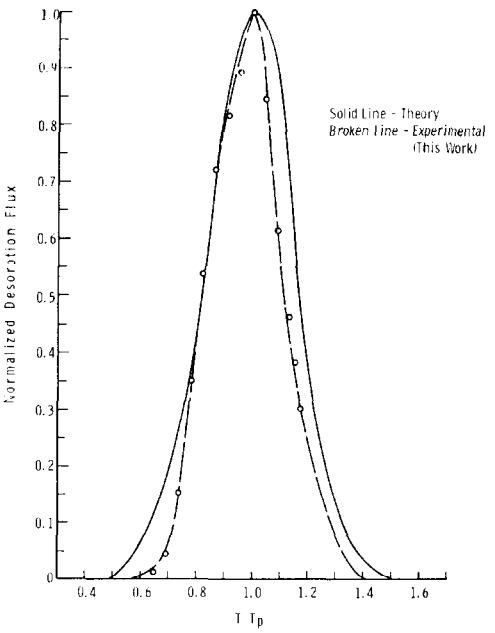

FIG. 12. Pyridine desorption from 10 wt% SiO_2/90 wt% Al_2O_3, theory versus experimental.

"the small pore diameters and large mean-free paths encountered during desorption." Thus, the apparent acid strength (activation energy for desorption) becomes very low. However, if one examines the characteristic time defined by $\tau_1 = (T_p - T_m)/\beta$ for the various samples, it is found that τ ranges from approximately 50 to 700 sec from the highest to the lowest heating rates used. Such long times are not consistent with any simple model of pore diffusion. A characteristic time $\tau_2 = (X_0)^2/D_K$ based on a Knudsen diffusion coefficient using the average pore radius for these samples and a mean diffusion distance equal to one-half the thickness of the sample give values of τ_2 of approximately 10^{-1} to 10^{-2} sec.

We cannot rule out some more complicated gas phase diffusion mechanism; but based on a surface diffusion mechanism, we may speculate on the transport of pyridine from the acid sites until it is detected in the gas phase. If the apparent energy that is measured corresponds to the activation energy for desorption, then the activation energy for surface diffusion, which is typically taken as one-quarter to one-half of this value, would result in a surface diffusion coefficient that was very weakly temperature dependent. The mean number of sites sampled by the pyridine during surface diffusion based on a Volmer hopping mechanism and using the values of τ_1 mentioned previously gives values of 10^5 to 10^6. This is a very small fraction of the total number of acidic sites present on the samples examined. Thus, a possible mode of transport once the pyridine has desorbed from its adsorption site is via a weakly activated surface diffusion mechanism. The increasing values of τ_1 with decreasing heating rate most likely represents the longer time spent traversing a given temperature interval; and the good agreement between the activation energies measured using the two techniques is the result of the insensitivity of the TPD spectra to readsorption as discussed by Cvetanovic. Further work is needed to clarify the mechanism of the pyridine desorption process.

CONCLUSIONS

A new, combined technique was successfully developed which permits simultaneous infrared examination and temperature-programmed desorption analysis by MS of a vapor base from microporous catalysts. Good agreement was obtained between activation energy for pyridine desorption calculated from (1) IR spectra and (2) the MS in a TPD analysis.

This combined technique was used to establish the kinetics of and mechanism for pyridine desorption from silica–alumina gel catalysts covering a wide range of composition. More detailed information about number, type, and strength of acid sites on catalysts can be obtained with this experimental approach. For a 90 SiO_2/10 Al_2O_3 by weight Xerogel the activation

energies for desorption of pyridine from Lewis and Brønsted sites are found to be only 5.3 and 7.2 kcal/mole, respectively.

APPENDIX I

Catalyst Wafer Preparation for Infrared Study

The preparation of catalyst samples for use in the high-vacuum IR cells in the Perkin–Elmer 180 spectrophotometer involves three principal steps: (1) grinding of a sample to a fine powder, (2) preparation of a thin wafer, and (3) insertion of the wafer in a cell and the cell in the IR compartment.

(1) The grinding of a sample is done with a Norbide mortar and pestle. The ground catalyst is then passed through a 400-mesh throw-away nylon screen. The disposable screens avoid intersample contamination.

(2) From the 400-mesh powder, a thin 13-mm-diameter wafer weighing between 3 and 10 mg is pressed. Wafers are generally formed with as low a pressure as will produce a self-supporting sample that will also withstand the effects created by rapid evacuation, rapid pressure rises, and rapid heating and cooling. The anvil and plunger assembly made from 316 stainless steel and purchased from Perkin–Elmer is the principal tool in the formation of a wafer. However, because many sample compositions stick to stainless steel or are magnetic or carry a high static charge, it is necessary to devise special anvils and plungers from materials such as Teflon, Pyrex, and Nalgene. 3M Magic Tape on die faces is necessary for many materials. Other devices used successfully to remove sticking wafers have been degaussing coils, Tesla coils, and vibrators. To get a uniform smooth wafer, the fine powder must be spread evenly over the surface of the plunger; the anvil must be inserted and rotated approximately five turns each clockwise and counterclockwise; then the necessary pressure must be applied. Depending on the catalyst material, optimum wafer pressure varies from a few pounds per square inch up to 10,000 psig.

(3) Once a wafer is formed, it is carefully placed in a quartz holder. The holder is inserted in the furnace chamber of the IR cell through one window port. The window port is replaced, and the cell is placed in one compartment of the infrared spectrometer. The cell is then connected via conflat flanges to a quadruple mass spectrometer and pumped high-vacuum stem. Through the vacuum stem the cell can be rapidly pumped to low pressure and the sample then pretreated as desired.

ACKNOWLEDGMENTS

We would like to thank Dr. Thomas R. Hughes, Chevron Research Company, for his critical review of our manuscript and helpful comments.

REFERENCES

1. Parry, E. P., *J. Catal.* **2**, 371 (1963).
2. Basila, M. R., Kantner, T. R., and Rhee, L. H., *J. Phys. Chem.* **68**, 3197 (1964).
3. Basila, M. R., and Kantner, T. R., *J. Chem. Phys.* **71**, 1681 (1966).
4. Hughes, T. R., and White, H. M., *J. Phys. Chem.* **71**, 2192 (1969).
5. Hughes, T. R., White, H. M., and White, R. J., *J. Catal.* **13**, 58 (1969).
6. Schwarz, J. A., *J. Vac. Sci. Technol.* **12**, 321 (1975).
7. Cvetanovic, R. J., and Amenomiya, Y., "Advances in Catalysis," Vol. 17, p. 103. Academic Press, New York, 1967.
8. Redhead, P. A., *Vacuum* **12**, 203 (1962).
9. Ehrlich, G., "Advances in Catalysis," Vol. 14, p. 256. Academic Press, New York, 1963.
10. Ryason, P. R., *Rev. Sci. Instrum.* **44**, 772 (1973).
11. Kearby, K., Ph.D. thesis, Univ. of Illinois, 1937.
12. Hsieh, P. Y., *J. Catal.* **2**, 211 (1963).
13. Naono, H., Moori, K., and Morimoto, T., *Bull. Chem. Soc. Japan* **49**, 1772 (1976).
14. Richardson, R. L., and Benson, S. W., *J. Phys. Chem.* **61**, 405 (1957).
15. Takahashi, M., Iwasawa, Y., and Ogasawara, S., *J. Catal.* **45**, 15 (1976).